

Mechanical stress power measurements during high-power laser ablation

Mark A. Shannon^{a)}

Department of Mechanical and Industrial Engineering, University of Illinois at Urbana-Champaign, 1206 West Green Street, Urbana, Illinois 61801

Boris Rubinsky

Department of Mechanical Engineering, University of California at Berkeley, Etcheverry Hall, Berkeley, California 94720

Richard E. Russo^{b)}

Lawrence Berkeley National Laboratory, Berkeley, California 94720

(Received 19 December 1995; accepted for publication 3 July 1996)

Laser-induced stresses have been studied extensively to understand macroscopic phenomenon during high-power laser ablation of solids. Recently, a norm of stress times the rate of change in stress, similar to mechanical stress power, was monitored acoustically in the target and ambient medium during high-power laser-material interactions, and compared with stress measurements. This study investigates the relationship between stress and the stress powerlike measurements (P^*), and their dependence on laser energy, intensity, and spot size. The importance of different components of stress on the measurements is also considered. Results from ablation of aluminum targets by a 30 ns uv excimer laser are presented that show changes in P^* with laser energy coupling, and the dependence of P^* on laser intensity and stress components. Potential issues are raised for further study of stress power as a diagnostic tool of laser-material interactions and as a fundamental mechanism of laser-energy coupling. © 1996 American Institute of Physics. [S0021-8979(96)01520-4]

I. INTRODUCTION

High-power, short-pulsed laser-material interactions induce mechanical stresses in the target from thermal expansion and phase-change, recoil momentum and shock waves from the ablated mass leaving the target at high velocities, and radiation pressure at very high intensity. As a result of high stresses, brittle fracture, plastic deformation, and spallation of normally ductile materials have been observed during high-power laser-material interactions. Accordingly, laser-induced stresses and plume dynamics during high-power laser-material interactions have been studied extensively.¹⁻¹⁵ Stress measurements have been investigated to determine mass removal, displacement, and pressure.¹⁶⁻¹⁹ Shock wave detection in the medium²⁰ and stress waves in the target²¹ have been used to detect the onset of ablation. Although these measurements of laser-induced stresses reveal important information about specific phenomenon, they do not directly reveal the amount of laser energy that is mechanically coupled to the target.

The coupling of laser energy to solids can occur via different mechanisms: thermal, chemical, mechanical, and electromagnetic. The amount of energy coupled to the target depends on the laser's power, wavelength, and pulse duration; the target's physical and optical properties, surface morphology and geometry; and the surrounding medium's pressure and properties. The amount of absorbed laser energy is highly nonlinear, making complete and accurate experimental measurements and theoretical interpretations difficult. Recently, far-field acoustic measurements were

employed for studying laser energy coupling via mechanical stress power, which implicitly includes different mechanisms of energy transfer.²² The method relies on transient acoustic measurement of laser-induced stresses in the target and ambient medium while varying laser intensity. A form of mechanical stress power was monitored in the far field to determine if changes in laser-energy coupling in the near field could be detected during nano- and picosecond laser ablation of metals. Notable changes with laser intensity were reported in air, He, and Ar atmospheres at varying pressures. In a follow-up study,²³ stress power was compared with simultaneous measurements of stress, which showed that the responses differed significantly with laser intensity: stress power corresponded to changes in laser energy coupling in the target, whereas stress did not. This article addresses more completely the relationship between stress and stress power, as well as the dependence of stress power on laser intensity, and the affect of different components of stress on the stress power measured.

Stress power, P , is defined as

$$P = \mathbf{T} \cdot \mathbf{L}, \quad (1)$$

where \mathbf{T} is the Cauchy stress tensor $\tau_{ij} \mathbf{e}_i \otimes \mathbf{e}_j$, and \mathbf{L} is the velocity gradient tensor $\mathbf{L} = v_{i,j} \mathbf{e}_i \otimes \mathbf{e}_j$ ($i, j = 1, 2, 3$). The summation $\tau_{ij} v_{i,j}$ describes the mechanical power per unit volume arising from the dynamic deformation of a body under stress. P is large only if both the stress amplitude and the velocity gradient are large. P can also be a fundamental energy transfer mechanism that, depending on the material and the mode of dissipation, can heat the body, or can raise the kinetic energy of fracture and/or particles. For most laser-material interactions, P is very small with respect to the incident laser power per unit volume. However, P could be

^{a)}Electronic mail: mas1@uiuc.edu

^{b)}Electronic mail: rerusso@lbl.gov

come a significant mode of energy transport if the target is highly stressed over a very short time period. High-power, short-pulse lasers create precisely the type of loading that can cause P to be significant with respect to other modes of energy transport.

For this work, an average stress σ in piezoelectric transducers, which are located acoustically far from the laser-irradiation region, is measured over time. The average stress power in a linearly elastic transducer \bar{P} at time t is defined such that

$$\bar{P}(t) \equiv \bar{\sigma} \dot{\sigma} = 2CS\dot{S} = C \frac{d}{dt} (S^2), \quad (2)$$

where $S(t)$ is the acoustic emission signal, $\sigma(t) = gS(t)$, and $C = (1/2)\bar{\sigma}g^2$ is a proportionality constant. Therefore, $\bar{P}(t)$ in the transducer is a function of the stress and the rate of change in the stress. As a measure of the total stress power that acts on the transducer over an interval of time T , the mean power of an ergodic signal is calculated by integrating in the frequency, f , domain, such that

$$\begin{aligned} \frac{C}{T} \int \frac{d}{dt} [S(t)^2] dt &= \frac{C}{T} \int f \Sigma(f) \Sigma^*(f) df \\ &= \frac{C}{T} \int f |\Sigma(f)|^2 df, \end{aligned} \quad (3)$$

where $\Sigma(f)$ is the Fourier transform of $S(t)$, and Σ^* is the complex conjugate.

The transducer signal voltage results from an accumulation of charge at the electrodes due to the electric fields generated over the volume V of the transducer element. A quantity P^* is now defined as

$$P^* \equiv \int_V \left(\frac{C}{T} \int f \Sigma^2(f) df \right) dV = C^* \int f \Sigma^2(f) df, \quad (4)$$

where $C^* = CV/T$, and P^* has units of power. P^* is a mean norm of \bar{P} calculated from stress waves passing through the piezoelectric transducer element. Therefore, P^* is not a direct calculation of stress power as given in (1); rather it is a stress powerlike quantity calculated from transient stress-wave measurements.

In this work, the transducers are all located in the far field and record the linear elastic response of the transducer to stress-wave propagation. A substantial body of work exists in the literature on laser generated ultrasonic wave propagation in solids that can be referred to for probing laser-material interactions with acoustics.²⁴ For this work, transient measurements of acoustic waves in the far field were monitored to determine how changes in laser energy coupling to the target and surrounding medium affected measurements of P^* . Data are presented for P^* in a target, for P^* due to the pressure wave in the air above the surface, and for ratios of P^* from the individual stress components.

II. EXPERIMENTAL CONDITIONS

Stress power was studied versus laser energy, intensity, and spot size, and the target thickness. The mechanical response from the ablation was detected with three different

acoustic transducers to identify the separate stress wave carrying energy: the pressure wave in the ambient medium; the longitudinal and shear waves in the body of the target; and the Rayleigh waves that propagate along the surface of the target. Plate waves are ignored due to the short time periods involved and the relative stiffness of the target, transducer, and mount.

Aluminum (6061 Al in T6 condition) targets were ablated in air by using a 30 ns excimer laser at 248 nm wavelength. The surfaces are lapped flat to within 10 μm per cm, finished with 600 grit sandpaper, and preconditioned with approximately 100 laser pulses at $5 \times 10^6 \text{ W/cm}^2$. Aluminum was used due to its high coefficient of thermal expansion so that transducer sensitivity would not add noise and errors to stress power calculations at low laser intensities. The onset, magnitude, and power of the mechanical waves was measured to determine how the individual modes of transport change as a function of laser energy and intensity in these targets. Al targets 0.5, 1.0, 2.0, 3.0, 19.0, and 38.5 mm thick were ablated to determine if the thickness of the target produced any artifacts on the measurements by the body wave transducer due to mode conversion, scattering, and attenuation. Qualitative results from acoustically thin-to-thick targets remained the same, with only the magnitudes changing between the different thicknesses.

The experimental apparatus used for the experiments has been previously described.^{22,23} The following briefly describes the salient features. The laser used is a Questek model 2860 excimer laser ($\lambda = 248 \text{ nm}$) with a 30 ns pulse. Power attenuation was achieved through a combination of 25% and 50% beam splitters and energy output adjustment from 20 to 100 mJ/pulse. Beams were apertured to 6 mm diameter after the laser. A silicon photodiode was used to monitor energy for each laser pulse. The photodiode output was calibrated using a Moletron model PD-104 (NIST traceable) pulsed-laser power meter. The pulse-to-pulse variation was measured, and the data were normalized to the laser power. The laser beam was focused with a single quartz lens. The laser-beam spot size was altered by translating the lens with respect to the target. A new location on the target was used for each experiment. Intensity was calculated using the laser-beam spot size, pulse energy, and pulse duration. The spot sizes were determined by measuring the burn and ablation patterns on uv burn paper, and by comparing the burn patterns with the crater profile.

A 1-in.-diameter acoustic emission transducer (AET) with a -3 dB frequency response from 10 kHz to 18 MHz was placed at the rear of the target along the center line of the irradiated spot to detect longitudinal and shear waves propagating through the target. A 1/2-in.-diameter 1 MHz Panametrics transducer mounted on a Panametrics 45° shear wave wedge for aluminum, was placed 4 cm from the center of the spot to detect longitudinal, shear, and Rayleigh waves propagating along the surface of the material. Although the Rayleigh wave angle for Al is approximately 69° and the angle for transmitting longitudinal waves is less than 30° , the 45° wedge had a sufficiently large solid angle with respect to the source at the 4 cm placement that all modes at the surface could be detected with the same transducer. Both transducers

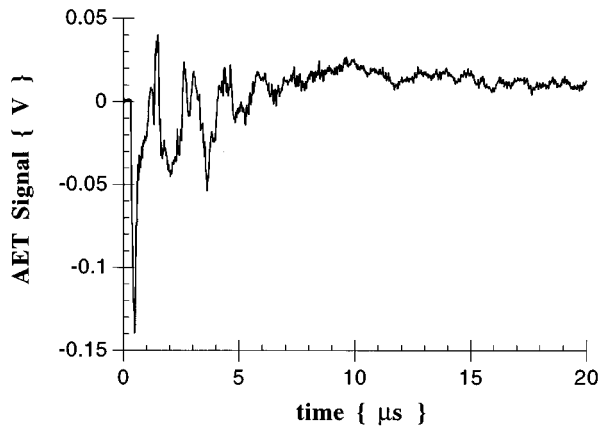


FIG. 1. Representative trace from the AET transducer of stress waves propagating through a 2 mm thick Al target being ablated with a 30 ns, 248 nm excimer laser. Laser beam is focused to a 1 mm diam spot size, with energy of 20 mJ/pulse.

were mounted with a thin layer of Dow Corning silicone vacuum grease. A Valpey–Fisher (VP-1093) 0–1.2 MHz Pinducer was placed 5 mm from the surface along the center line normal to the spot to detect the pressure wave propagating through the air. The data were captured with a Tektronix model 602A 2 Gsample/s digitizing oscilloscope. The peak frequencies and pressures recorded in the far field were well within the limits of the transducers, and the data acquisition exceeded the Nyquist criteria by at least a factor of 3.

For most experiments, only the first 20 μs of acoustic data were recorded for analysis. A representative signal from the AET transducer during ablation of the 2 mm Al target is shown in Fig. 1. The first longitudinal reflections reach the AET after approximately 1 μs and the first shear waves after 2 μs . Multiple reflections with mode conversion occur in a time period greater than 200 ms. Scattering occurring in the near field will lengthen the time period for all waves reaching the transducer. The initial response had decayed by 20 μs before additional reflections and plate vibrations occurred.

III. RESULTS

The data in Fig. 2(a) show the log of the calculated stress power vs the log of the laser intensity during ablation of the 2 mm Al target using eight different laser spot sizes over 16 different laser energies. The stress power, P^* , follows a power law dependence

$$P^* = cI^m, \quad (5)$$

with a distinct coefficient c and exponent m for each spot size. Even though the laser intensity increases orders of magnitude by reducing the spot size, P^* recorded at equal laser energies does not. P^* has only a weak dependence on area at the highest laser energies for spot sizes less than 3 mm, as depicted by the upper energy curve in Fig. 2(a). For equal laser energies, the base level of P^* increases nearly an order of magnitude for spots size below approximately 1 mm in diameter, as seen by the lower energy curve in Fig. 2(a).

Another way to show the effect of laser spot size on stress power measurements is to normalize P^* to the laser beam area, as shown in Fig. 2(b). The data for the log of

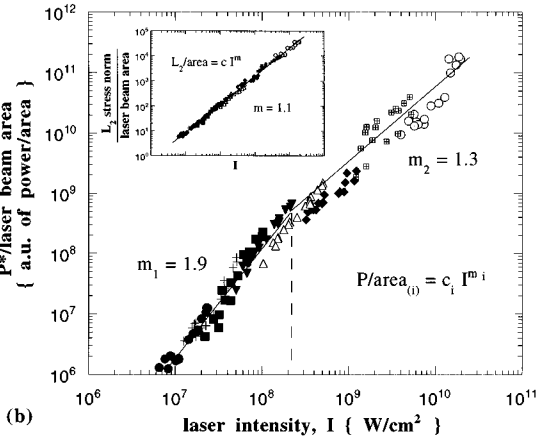
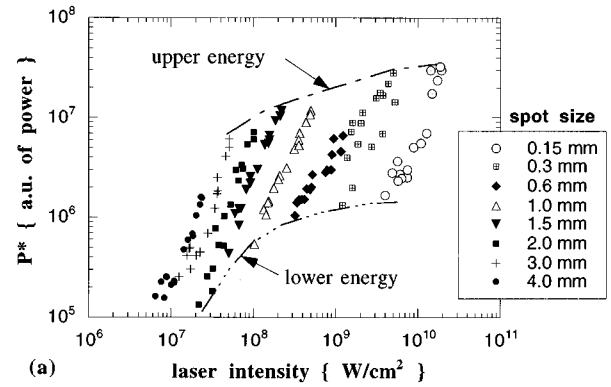


FIG. 2. (a) P^* calculated from the AET transducer from excimer laser ablation of a 2 mm thick Al target. The laser intensity, I , was varied by changing the nominal incident energy 16 times from 20 to 100 mJ/pulse, over 8 different laser spot sizes. The dotted curves bound equal upper (---) and lower (---) energies. (b) $P^*/\text{laser area}$ is plotted, showing two distinct regions of dependence. Inset shows the near linear dependence of the L_2 stress norm on I .

$P^*/\text{laser area}$ vs log of the laser intensity fall on the same curve, with two distinct regions. $P^*/\text{laser area}$ in each region follows a power law dependence as in Eq. (5), with an approximate quadratic ($m=1.9$) dependence below about $2 \times 10^8 \text{ W/cm}^2$ and larger than linear ($m=1.3$) dependence above the roll-off point of $2 \times 10^8 \text{ W/cm}^2$. Note that stresses per unit laser area do not show the same dependence on the laser intensity as stress power per unit area. The inset in Fig. 2(b) shows that the L_2 norm (root mean square) of the stresses divided by the laser beam area exhibits nearly linear ($m=1.1$) dependence over this same intensity range. The stress dependence is less than the P^* dependence over this range of laser intensity. These observations do not depend on the norm used for stress; maximum stress values showed the same results as the L_2 norm, except that the maximum stresses showed more scatter in the data.

Representative transducer response for the pressure waves in air are shown in Fig. 3(a) for ablation of the 3 mm thick Al target, using 0.3, 1, and 3-mm-diameter laser spot sizes. The magnitude and the speed of the shock wave increases, indicating the velocity and pressure of the gas behind the shock has increased. The 3 mm spot size wave

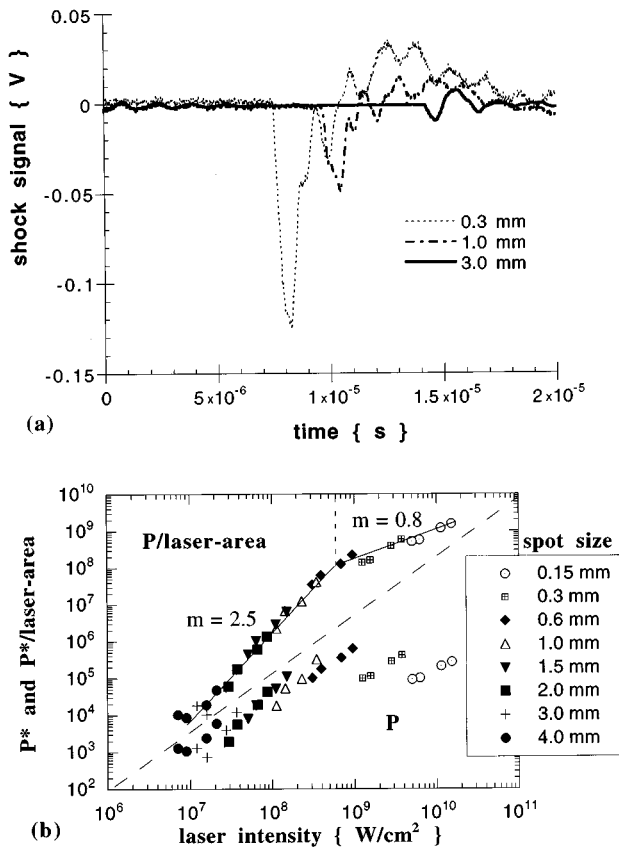


FIG. 3. (a) Representative traces of the transducer signals for pressure waves in air from excimer laser irradiation of 3 mm Al target. Laser focused to 0.3, 1.0, and 3.0 mm diam, with energy at 20 mJ/pulse. (b) The bottom shows P^* plotted vs laser intensity for eight spot sizes and four different energies ranging from 20 to 100 mJ/pulse. The top shows the plot of $P^*/\text{laser area}$ vs intensity.

speed corresponds with the speed of sound in air. From these shock data, P^* in air is calculated and plotted in the bottom of Fig. 3(b) as a function of the laser intensity for four different energy levels at each of the eight different spot sizes. P^* in the shock waves shows a similar pattern as in Fig. 2(a), except that the base line shift for spot sizes less than 1 mm is two orders of magnitude. For spot sizes ≥ 2 mm and laser energy of 20 mJ, P^* in air is at a minimum, since the pressure wave is propagating at the speed of sound. For spot sizes < 1.5 mm and/or at higher laser energy, the pressure wave greatly increases, and travels faster than the sound speed. As laser energy increases, the power of the shock increases, but not uniformly. P^* reaches a maximum for the 0.6 mm spot size, and then decreases as the laser intensity is increased by reducing the spot size. $P^*/\text{laser area}$ for the shock wave in air exhibits similar behavior to that in the target [Fig. 2(b)]: it collapses to one curve with two distinct regions. However, the intensity at the roll-off point differs (6 vs 2×10^8 W/cm²), and the slopes above roll off differ (0.8 vs 1.3).

The ratio of stress power in the medium to that in the target provides an explicit measure of how the shock power affects the stress power. The log of $P^*_{\text{medium}}/P^*_{\text{target}}$, simultaneously measured for the 3 mm thick Al target, is shown as

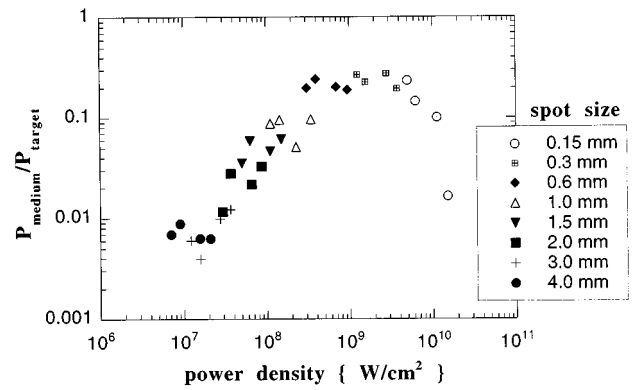


FIG. 4. The ratio of the P^* in the air medium over that in the 3 mm Al target is plotted vs laser intensity.

a function of the log of the laser intensity in Fig. 4. The ratio increases until about 5×10^8 W/cm², at which point it begins to roll off. A plateau is reached and then the ratio decreases above 4×10^9 W/cm². Two features are noteworthy: (i) below 10^8 W/cm² the medium and target stress power are closely linked, and (ii) above 5×10^8 W/cm², the coupling of mechanical power dramatically changes, with the target vs the medium gaining in stress power as laser energy increases, even for the same spot size.

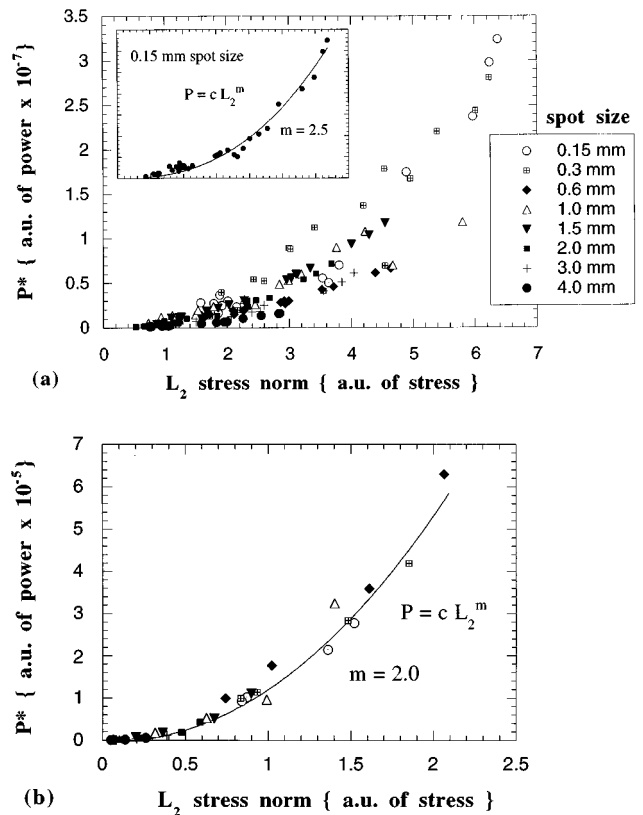


FIG. 5. The dependence of P^* on the L_2 stress norm is shown for the (a) target and (b) medium. Inset in (a) shows P^* vs L_2 over 32 laser energies for the smallest laser spot size.

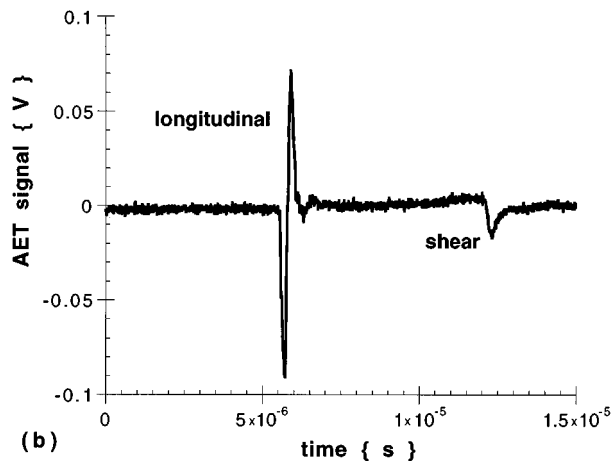
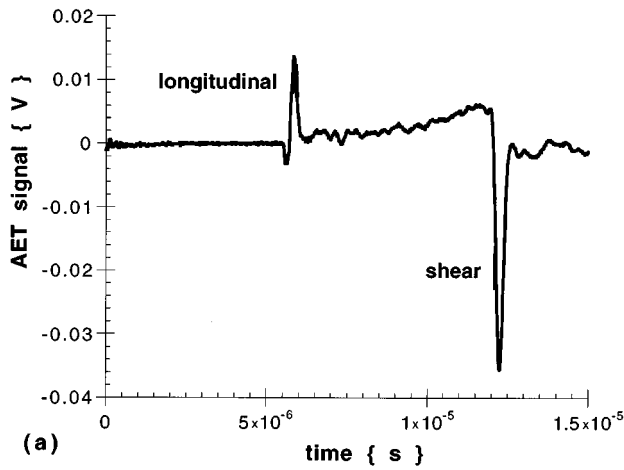


FIG. 6. Representative trace of AET transducer showing longitudinal and shear waves propagating in a 38.5 mm thick Al target. Laser beam is focused to (a) 3 mm and (b) 1 mm diam with incident energy at 20 mJ/pulse.

To demonstrate how stress power varies with the stress, P^* is plotted in Fig. 5 vs the L_2 norm of the stresses in the target (a) and the atmosphere (b). For the eight laser-beam spot sizes, P^* increases faster than stresses with laser energy. The rate of change in P^* vs L_2 increases as the spot size decreases. The inset of Fig. 5(a) shows a power law dependence for P^* with respect to L_2 over 32 energy levels, with $m=2.5$ for the smallest size of 0.15 mm. The lowest rate was found for the 4.0 mm spot size with $m=2.0$. Since $m > 2$ in every case, P^* increases faster than the stresses with laser intensity, with the greatest affect at the higher laser energies and smaller spot sizes.

The partitioning of stress power between the individual stress waves is studied using an acoustically thick Al target. The stress waves observed were the longitudinal wave in the target and at the surface, the body and surface shear waves, and the Rayleigh surface waves (plate waves are negligible). Representative traces of bulk longitudinal and shear waves for laser-beam spot size of 3 and 1 mm, and energy of 20 mJ/pulse are shown in Fig. 6. The magnitude of the shear wave is much greater than the longitudinal wave for the 3 mm spot size [Fig. 6(a)], whereas the situation is reversed for the 1 mm spot size [Figure 6(b)]. The magnitude of the longitudinal wave is 16 times greater for the 1 mm vs 3 mm spot

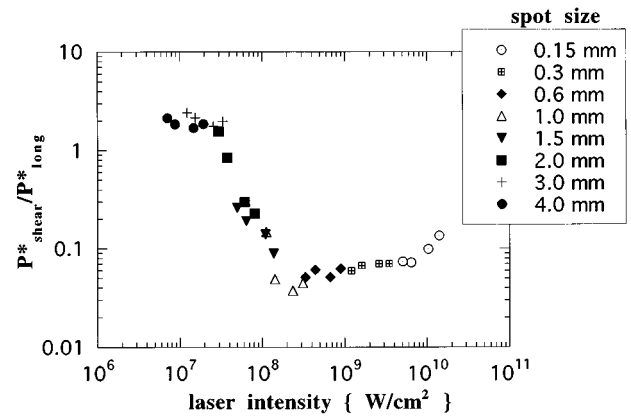


FIG. 7. The ratio of $P^*_{\text{shear}}/P^*_{\text{long}}$ vs laser intensity is plotted for eight spot sizes, with four energy levels each.

size; the shear wave magnitude is slightly less at 1 mm vs 3 mm. Therefore, the longitudinal wave grows rapidly with increased laser intensity, whereas the shear wave does not. The ratio of stress power of the shear (P^*_{shear}) to longitudinal (P^*_{long}) waves shown in Fig. 7 decreases with intensity until about $2 \times 10^8 \text{ W/cm}^2$. The ratio levels off and slightly rises as intensity increases further. $P^*_{\text{shear}}/P^*_{\text{long}}$ follows a similar but inverse pattern as that observed for $P^*_{\text{medium}}/P^*_{\text{target}}$ in Fig. 4.

Rayleigh waves were monitored to estimate the relative power of the stress components in the plane of the surface. Figure 8(a) shows representative traces of longitudinal, shear, and Rayleigh waves at the target surface for 3 and 1 mm spot sizes, at 20 mJ/pulse. The magnitude of the Rayleigh wave is approximately four times larger than the longitudinal wave at the surface. The shear wave is vanishingly small for the 3 mm spot size, and is much less than the Rayleigh wave for the 1 mm spot size. The ratio of P^* of the Rayleigh to longitudinal ($P^*_{\text{Ray}}/P^*_{\text{long}}$) waves in Fig. 8(b) shows that the power carried by surface vs bulk waves decreases with laser intensity until about $2 \times 10^8 \text{ W/cm}^2$ before leveling off. This behavior is similar to the shear vs longitudinal wave ratio shown in Fig. 7.

IV. DISCUSSION

Examination of Figs. 2(a) and the bottom of 3(b) shows that P^* versus laser intensity depends on the laser spot size, with P^* following a new curve in each case. However, normalizing P^* with the laser spot size in Figs. 2(b) and the top of 3(b) shows that the data collapse to one curve. $P^*/\text{laser area}$ as measured is a stress power flux that accounts for the finite size laser beam creating the loading, and is the desired quantity for determining the functional dependence on laser intensity.

The dependence of $P^*/\text{laser area}$ on laser intensity shows two distinct regions, both in the target and in the medium. In the Al targets, below about $2 \times 10^8 \text{ W/cm}^2$ $P^*/\text{laser area}$ has a near quadratic dependence ($m=1.9$) on laser intensity. This quadratic dependence is consistent with an elastic response during linear thermoelastic expansion and

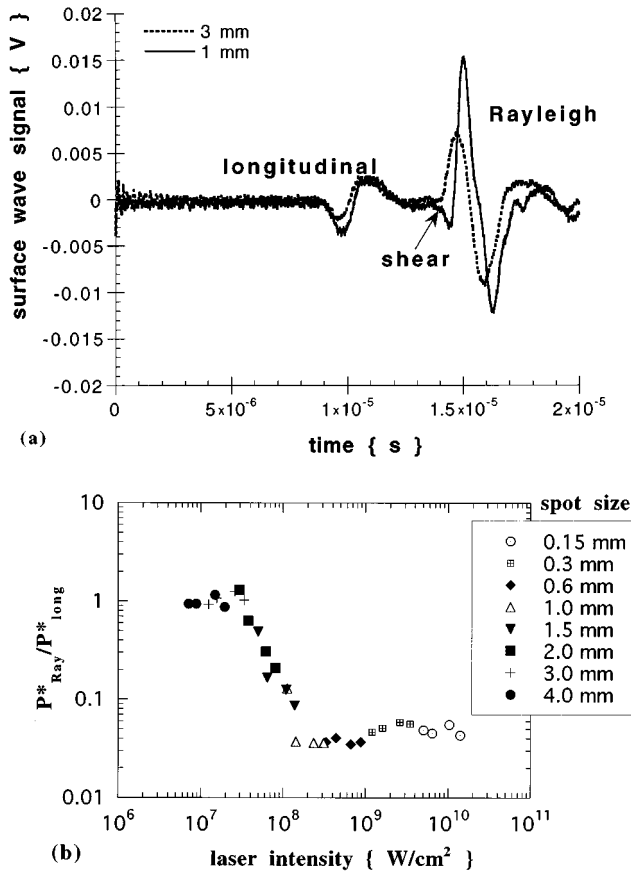


FIG. 8. The representative trace from the surface wave transducer shows in (a) the longitudinal, shear, and Rayleigh waves propagating at the surface of the 38.5 mm thick Al target. Laser spot sizes are 1 and 3 mm and energy is 20 mJ/pulse. The ratio P_{Ray}^*/P_{long}^* vs intensity is shown in (b) for eight laser spot sizes, at four energy levels each.

heating, and thermal evaporative models for pressure recoil predict a quadratic dependence of P^* vs laser intensity. For the Al target above 3×10^8 W/cm², $P^*/\text{laser-area}$ dependence on intensity shows a marked decline to $m=1.3$. This reduction is significant since the *stress* data itself does not show a reduction, and the point of roll off in the $P^*/\text{laser area}$ with laser intensity coincides with roll off observed in mass removal rates.²⁵

In the air medium above the target, the $P^*/\text{laser area}$ shows greater than quadratic dependence before roll off in the lower laser intensity regime. Linear thermal theory predicts a recoil pressure dependence of $m=2$. Development of a shock wave in the gas acts to increase the $P^*/\text{laser area}$ in the medium further, such that m would be >2 . However, above about 6×10^8 W/cm² m is <1 . This decrease in m for the $P^*/\text{laser area}$ in the medium could be due to (i) reduction in mass ablated per unit laser energy, (ii) increase in the loading time per unit stress, and (iii) dissipation of the stress and/or shock waves. The data in Fig. 3(a) for the shock waves show that increases in the loading time are small, and so (ii) is probably negligible. However, (i) and (iii) are likely to be occurring since shock waves can cause significant dissipation, and reduction in mass/laser energy does occur at laser intensities above the observed roll-off points.²⁵

The main contributors to the power carried mechanically by stress need to be established to determine the usefulness of monitoring particular components, as well as in investigating the laser ablation process itself. The sources of stress that dominate these laser-material interactions are thermal expansion in the target, vapor recoil, and shock wave generation in the gas medium. The temporal data for the thick target in Fig. 6 shows that the magnitude of the longitudinal wave grows much more rapidly than the shear wave with decreasing spot size. The longitudinal wave is strongly affected by vapor recoil and shock wave generation, as expected for normal loading, and the shear wave is most influenced by thermal expansion, as expected for constrained in-plane loading. The surface wave results from both expansion and normal loading, but is strongest with point normal loading, as seen in Fig. 8(a) as the spot size is reduced.

At higher laser intensities where stress power response significantly deviates from that of stress, P^* from longitudinal wave dominates that from shear and Rayleigh waves, as seen in Figs. 7 and 8(b). This growth in the longitudinal component of stress waves in the target corresponds with recoil and shock wave generation in the medium, as seen in Fig. 3(a) for decreasing spot sizes. However, the actual magnitudes of shear and Rayleigh waves do not decrease. Rather, they do not increase at the same rate as the longitudinal component until a plateau is reached, at the same point as roll off is observed. The plateau indicates that P_{long}^* either decreases or dissipates with respect to shear and Rayleigh, though it still is the dominant power component. Both P_{long}^* and P_{medium}^* are strongly affected by recoil and shock wave generation in the medium. Before roll off is reached, the target and medium stress power grow together linearly, as seen in the $P_{medium}^*/P_{target}^*$ ratio in Fig. 4. After roll off, the rate of growth of P_{long}^* and P_{target}^* decreases with laser intensity, though not at the same rate, indicating that laser energy coupling with both the target and medium is changing as well.

A significant result of this study is that P^* differs significantly from laser-induced stresses as a function of laser intensity. The stresses in the target increase almost linearly with laser intensity, but P^* increases quadratically at first, then slows above an observed roll-off point. Of value for monitoring complicated laser energy coupling into a target is that stress power, P , is directly related to a general energy balance, and stress is indirect.^{22,26} Although P^* is a stress powerlike quantity, and not P , changes in P^* reflect changes that occur to laser energy coupling with the target, even when stress measurements do not reflect that change.

The effect of laser energy coupling on stress power arises from the dependence of the velocity gradient and, thus, P , on stress. The effect of stress on stress power generation in the target and medium is seen in Fig. 5. P^* increases greater than quadratically as a function of the L_2 stress norm in the target, and quadratically in the medium. In the target, P^* vs L_2 depends weakly on the laser spot size. At the largest spot sizes, P^* is quadratic and at the smallest it grows by 2.5. As laser intensity increases and, thus, the stress imposed locally by the incident beam, the stress power increases at an even higher rate. In the medium, no area de-

pendence of P^* vs L_2 was observed. An issue in comparing P^* and stress is that P becomes more significant as stress increases, which was observed. Note that for $P = \tau_{ij}v_{i,j}$, only if $v_{i,j}$ is independent of τ_{ij} will P be proportional to L_2 . However, in general v_{ij} is a function of τ_{ij} , which depends on the constitutive relation linking stress and strain. For instance, if $v_{i,j}$ is a linear function of τ_{ij} , then P will be quadratic with stress. This behavior was observed for the intensity region studied. In a rapidly expanding gas medium, $v_{i,j}$ is a function of the pressure. At high pressure, the velocity gradient in the expanding gas depends on the velocity of the expansion front, and the pressure behind the front. The pressure p supplies the normal stress τ_{11} measured. Therefore, the stress power will be at least quadratic with the pressure, which is consistent with the observations seen in Fig. 5(b) for a normal shock.

Even though stress measurements do not explicitly show a change in laser energy coupling, a correlation should exist between the laser-induced stress and the energy transferred to the target. As laser energy coupling with a target changes, the amount and velocity of the ablated mass, and, thus, the stress from vapor recoil and shock wave generation varies. The ratio of $P_{\text{medium}}^*/P_{\text{target}}^*$ in Fig. 4 combined with Fig. 3(b) suggests that above the roll-off point at 3×10^8 W/cm², the rate of change of mass flux into the medium is decreasing, but the energy of the ablation products is increasing. Figures 2, 3, and 4 show that above 3×10^8 W/cm², P_{target}^* increases at a much larger rate than P_{medium}^* . If P_{target}^* is primarily due to longitudinal loading from the expansion plume as the data suggests, then if the mass flux drops, the mean velocity of the ablation products must be increasing to maintain the pressure increasing P_{target}^* . An increase in absorption of laser energy directly by the laser-induced plume is one mechanism that can reduce the amount of energy reaching the surface, thereby reducing the mass ablated, yet increasing the kinetic energy of the plume by increased heating. Shielding of the laser beam from the target by plasma formation, or plasma shielding, is consistent with these stress power results. More complicated plume dynamics may also play a role in the partitioning of medium and target stress power. Further study is needed to determine the cause of roll off in P^* without a concurrent roll off in stress.

V. CONCLUSION

This research is an initial investigation for utilizing the concept of mechanical stress power caused by laser-induced stresses in a target and in the ambient medium to investigate laser ablation of solid materials. At high intensities with short pulses, the stresses imposed on a target are substantial, and stress power should not be ignored when considering an energy balance for the laser-material interaction. Future research on stress power during laser-material interactions will determine its relative importance as laser intensities continue to increase, and for studying laser-material-plasma interactions during high-intensity laser irradiation. To do so, several issues still need to be explored.

The amount of energy coupled mechanically to the target needs to be established. The magnitude of P is determined

via the partitioning of energy that satisfies a general balance that includes thermal, mechanical, chemical, and electrical energy terms. The degree of partitioning depends on the constitutive relations for stress, strain, and heat transfer, as well as for internal energy. As P increases with respect to the total incident laser power, changes in energy transport might be expected to occur depending on the material and dissipation mechanisms, thereby limiting the mechanical propagation of energy. As such, the form and amount of mass ejected, as well as its kinetic energy, could change in the near field with changes in P . These initial experimental results indicate that measuring P^*/area in the far field reflects changes in energy coupling in the near field. In principle, stress power may be measured in the near field to investigate fundamental laser energy coupling mechanisms. However, much theoretical and experimental work remains for this to occur.

A unique result of these experiments is that P^* shows a distinct offset at the lowest laser energies. The base line stress power shifts an order of magnitude for small spot sizes due to shock wave generation. However, the initiation of the shock wave is the subject of continuing research, and it may be related to gas ionization breakdown, not merely expansion due to mass removal. Gas ionization breakdown at intensities as low as 10^8 W/cm² above a metallic surface is less than that observed with direct detection, yet an onset of ionization would help explain the offset. The sensitivity of P^* to changes in loading gives the method good potential as a laser diagnostic technique.

The frequency dependence for the power spectrum of P^* needs investigating. The values of P^* in this study are scalars independent of frequency. However, the power spectrum in the frequency domain changes with different laser loadings. Therefore, the power spectrum of P^* may reveal more information as to laser energy coupling mechanisms, both in the target and in the medium.

ACKNOWLEDGMENT

This Research was supported by the U.S. Department of Energy, Office of Basic Energy Sciences, Chemical Sciences Division, Chemical Separation and Analysis Branch, under Contract No. DE-AC03-76SF00098.

- ¹J. F. Ready, *Effects of High-Power Laser Radiation* (Academic, Orlando, 1971).
- ²J. Fournier, P. Ballard, P. Merrien, J. Barralis, L. Castex, and R. Fabbro, *J. Phys. (France) III* **1**, 1467 (1991).
- ³D. B. Geohegan, *Thin Solid Films* **220**, 138 (1992).
- ⁴G. Koren, *Appl. Phys. Lett.* **51**, 569 (1987).
- ⁵P. E. Dyer and R. Srinivasan, *Appl. Phys. Lett.* **48**, 445 (1986).
- ⁶G. A. Askar'yan and E. M. Moroz, *Sov. Phys. JETP* **16**, 1638 (1963).
- ⁷H. Wang, A. P. Salzberg, and B. R. Weiner, *Appl. Phys. Lett.* **59**, 935 (1991).
- ⁸F. J. Mayer and G. E. Busch, *J. Appl. Phys.* **57**, 827 (1985).
- ⁹J. C. S. Kools, T. S. Baller, S. T. De Zwart, and J. Dielman, *J. Appl. Phys.* **71**, 4547 (1992).
- ¹⁰R. Kelly and R. W. Dreyfus, *Nucl. Instrum. Methods Phys. Res. B* **32**, 341 (1988).
- ¹¹L. C. Yang, *J. Appl. Phys.* **45**, 2601 (1974).
- ¹²F. Cottet and M. Boustie, *J. Appl. Phys.* **66**, 4067 (1989).
- ¹³C. S. Speight, L. Harper, and V. S. Smeeton, *Rev. Sci. Instrum.* **60**, 3802 (1989).

- ¹⁴R. E. Beverly, III and C. T. Walters, *J. Appl. Phys.* **47**, 3485 (1976).
- ¹⁵F. Dahmani and T. Kerdja, *Laser Particle Beams* **9**, 769 (1991).
- ¹⁶E. Matthias, J. Siegel, S. Petzoldt, M. Reichling, H. Skurk, O. Kading, and E. Neske, *Thin Solid Films* **254**, 139 (1995).
- ¹⁷C. Stauter, J. Fontaine, and Th. Engel, *Appl. Surf. Sci.* **96**, 522 (1996).
- ¹⁸A. Hoffmann and W. Arnold, *Appl. Surf. Sci.* **96**, 71 (1996).
- ¹⁹L. Grad and J. Mozina, *Appl. Surf. Sci.* **69**, 370 (1993).
- ²⁰L. Balazs, R. Gijbels, and A. Vertes, *Anal. Chem.* **63**, 314 (1991).
- ²¹A. C. Tam and H. Coufal, *Appl. Phys. Lett.* **42**, 33 (1983). W. P. Leung and A. C. Tam, *ibid.* **60**, 23 (1992).
- ²²M. A. Shannon and R. E. Russo, *Appl. Surf. Sci.* **96**, 149 (1996).
- ²³M. A. Shannon and R. E. Russo, *Appl. Phys. Lett.* **67**, 3327 (1995).
- ²⁴C. B. Scruby and L. E. Drain, *Laser Ultrasonics* (Adam Hilger, Bristol, 1990); F. Bunkin, A. A. Kolomensky, and V. G. Mikhalevich, in *Laser Science and Technology*, Vol. 12 (Harwood Academic, Chur, Switzerland, 1991); S. J. Davies, C. Edwards, G. S. Taylor, and S. B. Palmer, *J. Phys. D* **26**, 329 (1993).
- ²⁵M. A. Shannon, X. L. Mao, A. Fernandez, W. T. Chan, and R. E. Russo, *Anal. Chem.* **67**, 4522 (1995).
- ²⁶M. A. Shannon, Ph.D. dissertation, University of California at Berkeley, 1993.